Journal of Power Sources 213 (2012) 106–111

Contents lists available at SciVerse ScienceDirect

Journal of Power Sources

journal homepage: www.elsevier.com/locate/jpowsour

Three-dimensional porous nano-Ni supported silicon composite film for high-performance lithium-ion batteries

Y.Q. Zhang, X.H. Xia, X.L. Wang*, Y.J. Mai, S.J. Shi, Y.Y. Tang, C.G. Gu, J.P. Tu*

State Key Laboratory of Silicon Materials, Department of Materials Science and Engineering, Zhejiang University, Hangzhou 310027, China

ARTICLE INFO

Article history:
Received 9 February 2012
Received in revised form
11 March 2012
Accepted 28 March 2012
Available online 7 April 2012

Keywords:
Amorphous silicon
Magnetron sputtering
Hydrogen bubble template
Porous film
Lithium-ion battery

ABSTRACT

A three-dimensional (3D) porous nano-Ni supported Si composite film is successfully fabricated by the combination of hydrogen bubble template electrodeposition of porous nano-Ni film and radiofrequency magnetron sputtering amorphous silicon. As anode for lithium-ion batteries, the 3D porous Ni/Si composite film shows noticeable electrochemical performance with high capacity of 2444 mAh g^{-1} at a current density of 0.84 A g^{-1}, superior capacity retention of 83% after 100 cycles, as well as excellent rate capability with 1420 and 1273 mAh g^{-1} at charge–discharge current densities of 4.2 A g^{-1} and 8.4 A g^{-1} after 100 cycles, respectively. The enhanced electrochemical performance is mainly attributed to the highly porous conductive architecture, which provides good mechanical support and electron conducting pathway for active silicon and alleviates the structure degradation caused by volume expansion during the cycling process.

1. Introduction

There is great interest in developing high-performance rechargeable lithium batteries with high energy/power density and long lifespan for applications in portable electronic devices and electric vehicles [1–7]. Of the available candidate materials for lithium-ion batteries, silicon is the most promising and extensively studied anode material due to its low discharge potential (−0.5 V vs. Li/Li^+) and high theoretical capacity (4200 mAh g^{-1} an order of magnitude beyond that of conventional graphite) [8,9]. Nevertheless, its practical application is restrained by the poor cycling stability resulting from the large specific volume change (volume change of 300–400%) causing pulverization and deterioration of active materials during cycling [10]. To overcome these drawbacks, previous studies heavily focused on Si active/inactive matrix composites [11–16]. Particularly, preferably Si–carbon composites have been widely investigated and improved performances have been demonstrated [17,18]. Despite this progress, it still leaves much space for achieving the satisfactory cycle performance and high-rate capability of Si-based anode, particularly in terms of designing new high-performance Si-based electrode material.

Nanostructured porous Si films have been intensively investigated as building components in electrochemical energy storage and conversion devices because they provide short diffusion paths to ions and electrons, and alleviate the structure damage caused by volume expansion, leading to super cycle stability and high energy conversion efficiency [2,3]. Self-supported Si nanowires [19–23], nanotubes [24–26], and 3D macroporous films [27] have been synthesized and demonstrated to exhibit pretty good cycling stability since these porous structures provide enough space to accommodate Si volume changes resulting in enhanced electrochemical performance. More recently, great efforts are dedicated to designing new porous silicon/metal composite films, in which the porous metal structure can provide the space to accommodate the volumetric change of the active silicon whereas the additional component facilitates the electron collection and transport. Previously, Zhang et al. successfully demonstrated nickel nanocone-array supported silicon with enhanced electrochemical performance [28]. Besides, Guo et al. used a Cu–Si nanocable arrays directly grown on a current collector to realize high-performance anodes with excellent stabilities and high-rate capabilities [29]. The highly porous conductive metal (Ni or Cu) films not only act as an integrated current collector to enhance the electronic conductivity but also serve as a mechanical support and release the structural stress/strain associated with lithium-ion insertion/extraction processes.

In recent years, three-dimensional (3D) porous nano-metal films prepared by hydrogen bubble template have elicited much

* Corresponding authors. Tel.: +86 571 87952573; fax: +86 571 87952856.
E-mail addresses: wangxl@zju.edu.cn (X.L. Wang), tujp@zju.edu.cn, tujplab@zju.edu.cn (J.P. Tu).

0378-7753/$ – see front matter © 2012 Elsevier B.V. All rights reserved.
doi:10.1016/j.jpowsour.2012.03.052

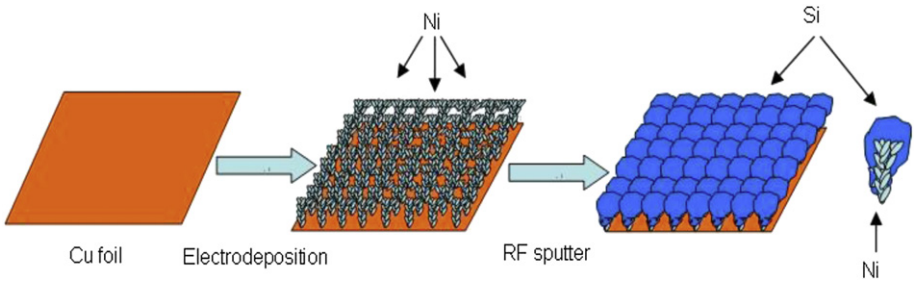

Fig. 1. Schematic diagram illustrating the fabrication of 3D porous nano-Ni film supported silicon anode architecture.

interest due to their distinctive structural features and intriguing properties. These 3D porous nano-metal films show highly porous dendritic walls composed of numerous nanoparticles, possessing extremely high surface area and open porous structure. To date, several 3D porous nano-metal films have been synthesized by hydrogen bubble template [30–32]. More recently, our group has used 3D porous nano-Ni film as scaffold to fabricate 3D porous nano-Ni/$Co(OH)_2$ composite film for supercapacitor with superior electrochemical properties [33]. Inspired by these results, herein, we synthesized a novel porous-structured Si electrode: 3D porous nano-Ni film supported Si film (3D porous Ni/Si) for lithium-ion battery application. Fig. 1 illustrates a typical preparation procedure of the electrode. In our case, the electrodeposited 3D porous nano-Ni film based on hydrogen bubble template acts as a backbone to deposit amorphous Si by radiofrequency (RF) magnetron sputtering method. The 3D porous Ni/Si anode exhibits impressive electrochemical performance with a high capacity, pretty good cycling stability and thus promising application.

2. Experimental

2.1. Preparation of 3D porous nano-Ni film

All solvents and chemicals were of reagent quality without further purification. The electrodeposition of 3D porous nano-Ni films was performed in a standard two-electrode glass cell at room temperature with electrolyte consisting of 2 M NH_4Cl and 0.1 M $NiCl_2$ at a pH value of 3.5, cleaned Cu foil with one side covered by

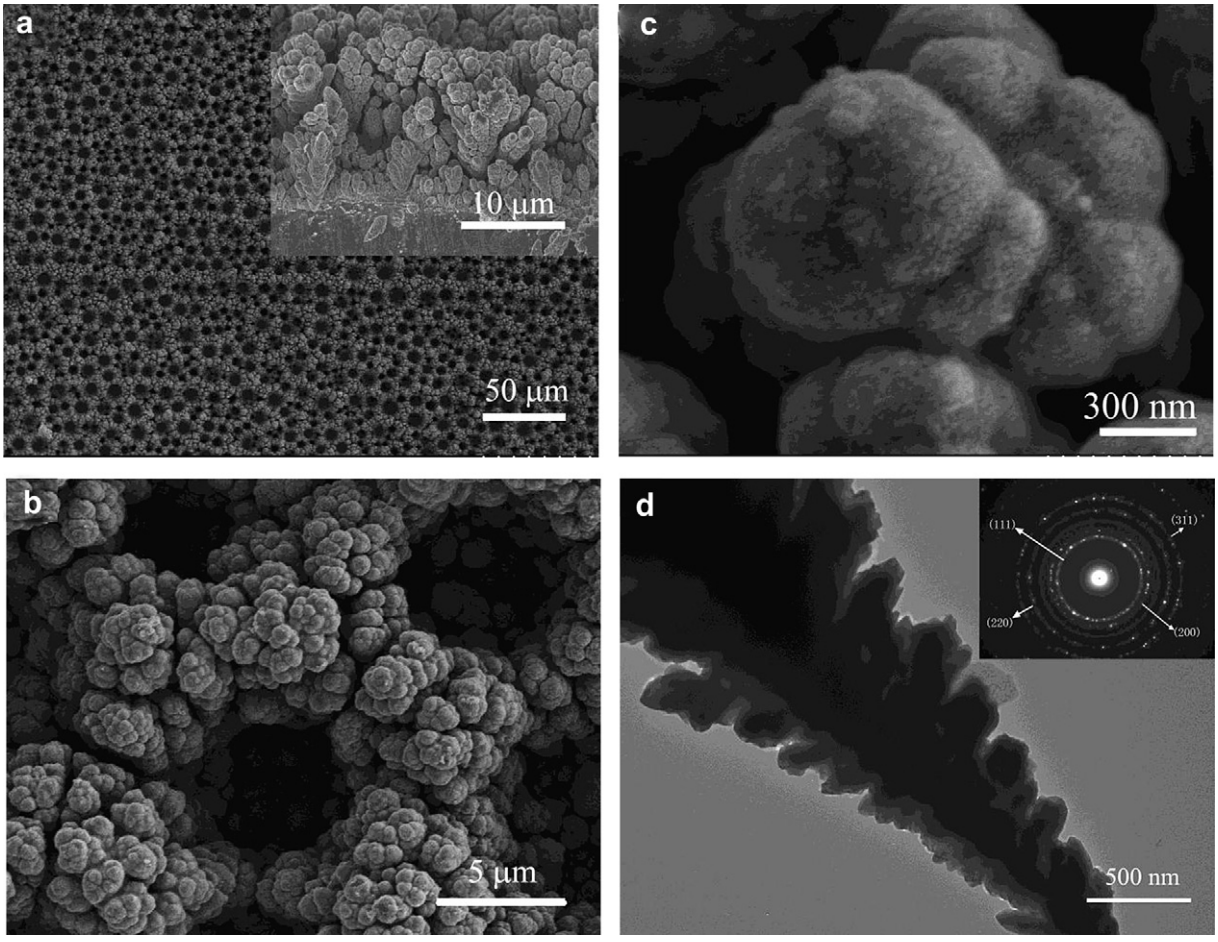

Fig. 2. SEM images of 3D porous nano-Ni film: (a) top and cross-sectional (inset) views, (b), (c) magnified SEM image; (d) TEM image of nano-Ni film.

insulting tapes as working electrode and a Pt foil as counter electrode. The distance between the two electrodes was 1 cm and the electrodeposition was carried out at a constant current density of 2 A cm^{-2} for 25 s. During the electrodeposition, the electrolyte was vigorously stirred by magnetic stirrer. Finally, the 3D porous nano-Ni films were washed with deionized water and dried in vacuum oven at 60 °C for 2 h. The loading density of Ni was about 2 mg cm^{-2}.

2.2. Fabrication of 3D porous Ni/Si electrodes

RF magnetron deposition of Si on the 3D porous nano-Ni film was carried out in argon (Ar)-filled environment at room temperature. Prior to deposition, the chamber was pumped down to a base pressure below 3×10^{-3} Pa while the work pressure was kept at 0.67 Pa. The distance between the target and the rotating substrate holder was held constant at 60 mm. Deposition of Si was conducted at a bias voltage of −100 V and a target current of 0.04 A. The average loading rate is determined to be 0.3 mg cm^{-2} in 1 h. In this experiment, the deposition of Si was carried out for 1 h.

2.3. Electrode characterization

The samples were characterized by X-ray diffraction (XRD, Rigaku D/max 2550-PC) and Raman spectroscopy (LABRAM HR-800). The morphologies of all samples were observed by field emission scanning electron microscopy (FESEM, FEI SIRION). For the transmission electron microscopy (TEM, JEOL JEM-200CX), the composite film was scratched from the Cu substrate and redispersed in ethanol solution.

2.4. Electrochemical measurements

The 3D porous Ni/Si grown on Cu foils was directly used as electrodes for electrochemical characterization. Coin cells (2025) were assembled in an Ar-filled glove box and lithium metal foil as the counter electrode, a polypropylene (PP) micro-porous film (Cellgard 2300) as the separator, 1 M $LiPF_6$ in ethylene carbonate (EC)–diethyl carbonate (DEC) (1:1 in volume) as the electrolyte. Cyclic voltammetry (CV) measurements were performed on a CHI660C electrochemical workstation (Chenhua, Shanghai) at room temperature. The galvanostatic charge–discharge tests were conducted on a LAND battery program-control test system.

3. Results and discussion

Self-supported 3D porous nano-Ni film is successfully prepared by a facile cathodic electrodeposition accompanying hydrogen evolution. The as-prepared Ni film exhibits a 3D porous structure with highly porous nanoramified walls. The feature size of the large pores in the Ni film is around 5–10 μm (Fig. 2a). The cross-sectional SEM image (inset in Fig. 2a) shows that the Ni walls consist of numerous dendrites forming a mechanically self-supported film and the thickness of the porous Ni film is approximately 10 μm. More importantly, the walls of the Ni film consist of numerous

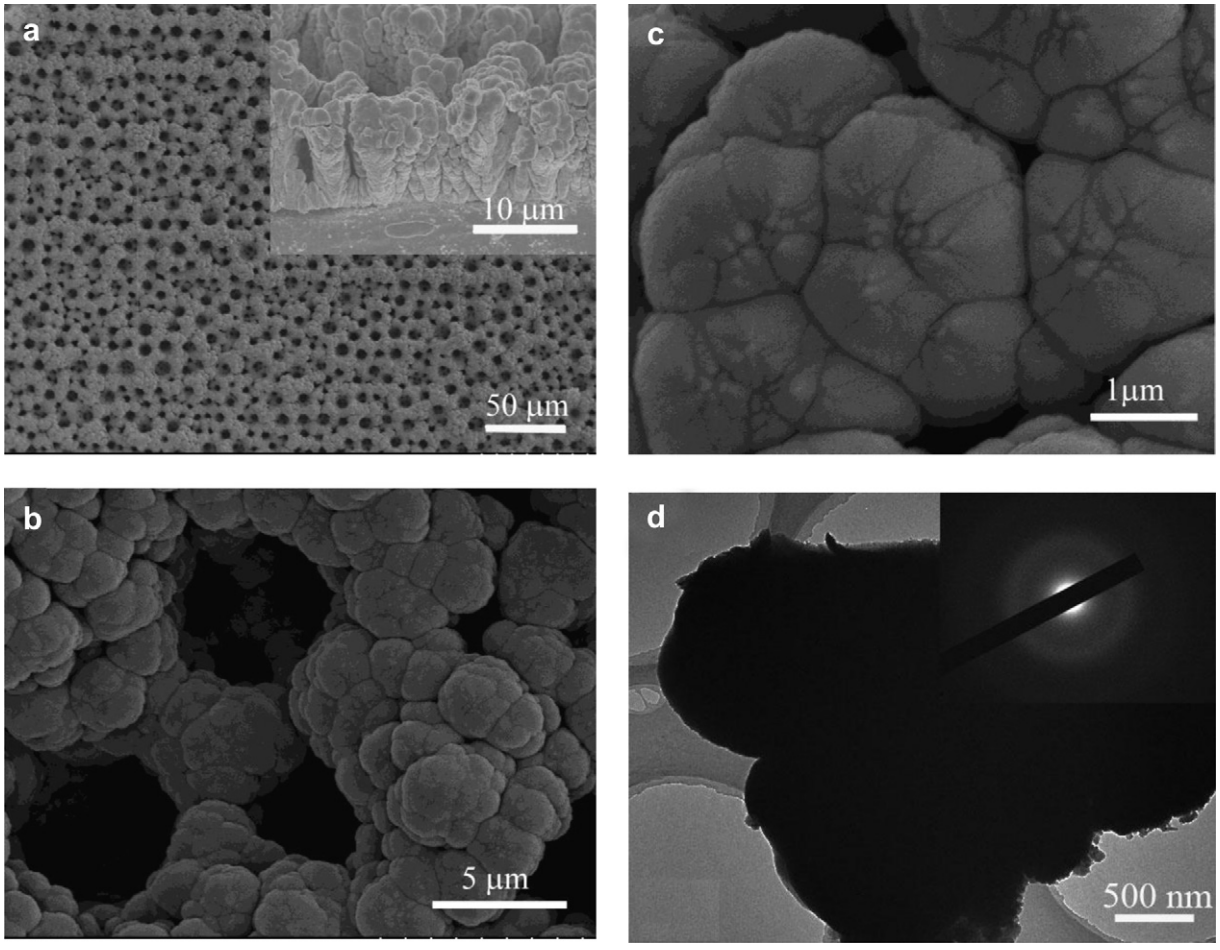

Fig. 3. SEM images of 3D porous Ni/Si film: (a) top and cross-sectional (inset) views, (b), (c) magnified SEM image; (d) TEM image of Ni/Si composite.

interconnected nanoparticles with diameters of 200–300 nm and show continuous nanopores ranging from 10 to 200 nm (Fig. 2b and c), which is further confirmed by TEM result (Fig. 2d). The selected area electronic diffraction (SAED) pattern reveals the existence of Ni phase with polycrystalline nature (inset in Fig. 2d). Obviously, the porous structure can make the nano-Ni film capture more silicon from different directions during the following sputtering deposition.

After deposition of Si, the Ni/Si film maintains the 3D porous structure (Fig. 3a and b). The surface of the 3D porous Ni/Si film becomes smooth. The Ni dendrites are wrapped by a layer of Si both on the top and side, resulting in a more compact appearance. Additionally, at high magnification (Fig. 3b and c), the continuous nanopores are disappeared and the Si layer shows convex morphology with caps of cone-shaped 'lattice'. According to the previous report [34], the convex morphology is able to release the internal stress formed during the physical deposition. Hence, it is expected that similar internal stress induced by lithium-ion insertion into silicon will be also easily released through this convex morphology. Furthermore, the 3D porous structure provides free space for stress releasing during lithium-ion insertion. Compared to the TEM image before Si deposition, the Si layer is uniformly covered on the porous nanoramified walls (Fig. 3d). And diffraction rings in the SAED pattern confirm the amorphous characteristics of Si.

The amorphous nature of silicon is further confirmed by XRD and Raman microspectroscopy (Fig. 4a and b). The typical peak of crystalline Si centered at 2θ degree of 28° is not identified [15,35]. All the diffraction peaks are attributed to the copper foil and electrodeposited nano-Ni. The Raman spectrum shows four broad spectra corresponding to four phonon bands: a broad transverse optical mode (TO) peak (~480 cm^{-1}), the longitudinal optical mode (LO) peak (400 cm^{-1}), the longitudinal acoustic mode (LA) peak (300 cm^{-1}) and transverse acoustic (TA) with a peak at 150 cm^{-1}, which are typical features of amorphous silicon vibration modes [36,37]. The band observed around 630 cm^{-1} corresponds to

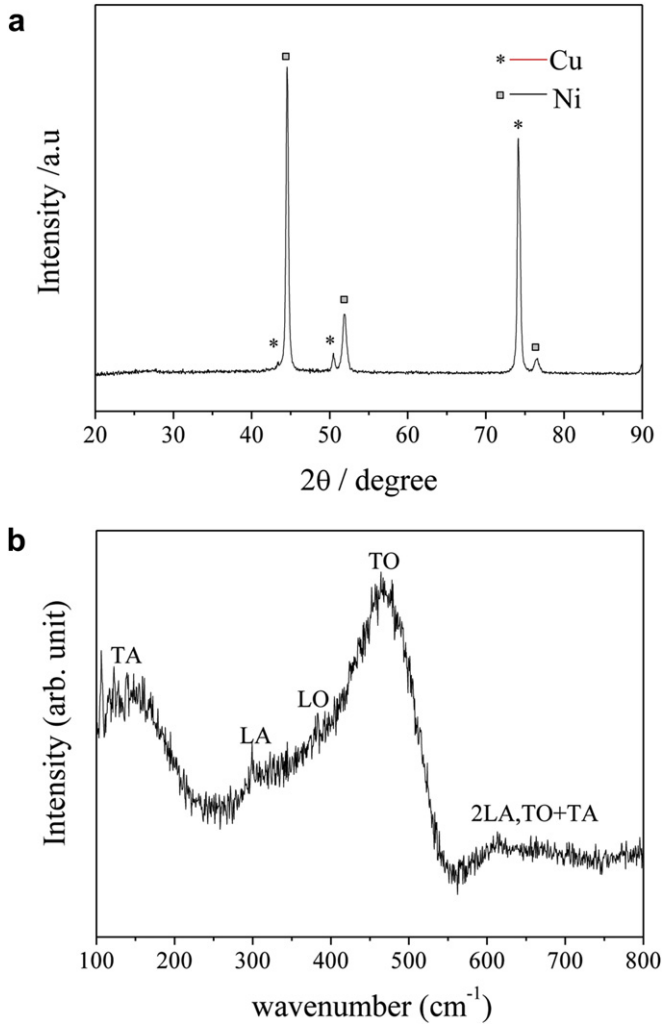

Fig. 4. (a) XRD pattern of 3D porous Ni/Si film, (b) Raman spectrum of 3D porous Ni/Si film.

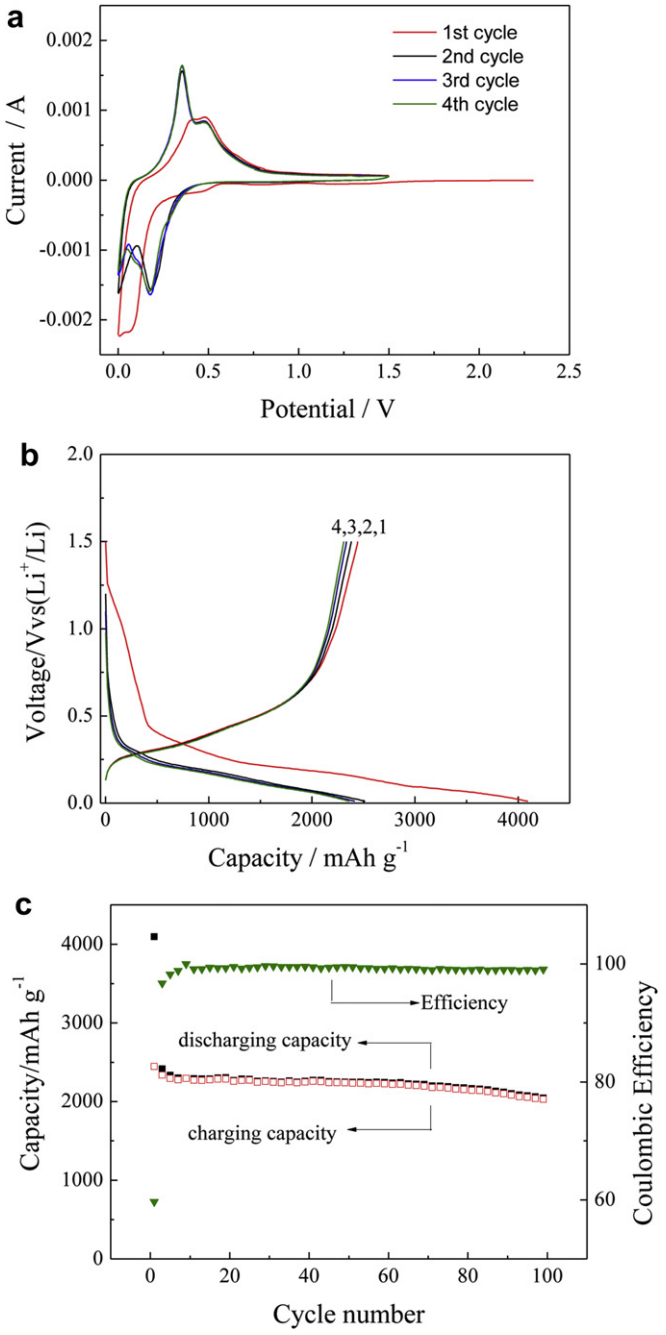

Fig. 5. (a) CV curves of 3D porous Ni/Si film electrode at a scanning rate of 0.1 mV s^{-1} (potential range: 0–1.5 V vs. Li^+/Li) for the first 4 cycles. (b) Voltage profiles of the electrode in half cells cycled between 0.01 V and 1.5 V at a current density of 0.84 A g^{-1}. (c) Cycling behavior for the half cells in (b).

the 2LA second order phonon Raman scattering and TO + TA overtone [38].

Fig. 5a shows the CV profiles of the 3D porous Ni/Si composite film in a potential window of 0–1.5 V (vs. Li^+/Li) at a scanning rate of 0.1 mV s^{-1} for the first 4 cycles. In the case of the first cathodic half-cycle, a broad cathodic peak at around 0.4 V could be attributed to the formation of a solid electrolyte interphase (SEI) film [28,39]. This peak disappears under the subsequent cycles meaning that no new SEI layer forms under subsequent process. Another cathodic peak appears at around 0.2 V and becomes quite large below 0.1 V, which can be ascribed to the formations of a series of Li_xSi alloys. After the first cycle, the above peak moves to 0.2 V. In the case of the first anodic process, two broader anodic peaks at 0.38 and 0.5 V correspond to the phase transition between amorphous Li_xSi and amorphous silicon, respectively. The intensity of the first anodic peak increases after the first cycle indicating improvement of Li extraction kinetics, while the second peak at 0.5 V, no matter shape or position, is similar to the subsequent cycles [40]. It may be due to the surface area changes of the 3D porous Ni/Si anode after the first cycle. CV behavior presents remarkably repeatable shapes after the first cycle suggesting high reversibility of the lithiation/delithiation reaction.

Fig. 5b shows the voltage profiles of the 3D porous Ni/Si anode between 0.01 and 1.5 V at a current density of 0.84 A g^{-1}. The sloping drop before 0.5 V might be the reaction of Li with SiO_x and NiO, which are introduced during the sample synthesis and battery assembly, even though they cannot be detected in Raman spectrum and XRD. Both of them are partly reversible in the voltage range of 0.01–1.5 V [29,41]. The short plateau at 0.40 V is the SEI formation potential on a Si surface [28,29]. This plateau disappears during the following cycles, which is in good agreement with CV measurement. The following sloping region gradually dropping to 0.01 V is related to the Si lithiation to amorphous Li_xSi. After the first cycle, the discharge and charge profiles show typical behavior (sloping curves) of Li intercalation/extraction into/from the amorphous Li_xSi [23,37,38].

The 3D porous Ni/Si anode shows rather good electrochemical performance in terms of both the specific capacity and cycling stability. As shown in Fig. 5c, the first discharge and charge capacities are 4095 mAh g^{-1} and 2444 mAh g^{-1}, respectively, with a low initial columbic efficiency of 60%. In addition to the formation of SEI film, the initial irreversible capacity can also be ascribed to a few SiO_x and NiO coverage as discussed above. The coulombic efficiencies are increasing gradually with, an efficiency of 94.6% in the second cycle. From 5th to 100th cycle, both the discharge and charge capacities keep a steady level and the coulombic efficiencies achieve as high as 98% and upwards. The charge capacity for the 5th cycle is 2292 mAh g^{-1} and that for the 100th cycle is 2025 mAh g^{-1}, leaving a retention rate of 88.3%, or 99.8% per cycle. The excellent cyclability is superior to previously reported Si active/inactive matrix composites [11,12,14,42] and comparable to those of recent research on novel nanostructures of silicon anodes (such as nanowires, nanotubes, nanorods, nest-like nanospheres, and three-dimensional porous particles) [8,19–22,24–26,43]. This excellent electrochemical performance of the Ni/Si composite is attributed to its unique 3D porous structure. The inactive 3D porous Ni matrix acts as the confining buffer to accommodate the enormous volume changes and alleviates the concomitant huge stresses owing to repeated Li alloying/dealloying with Si.

To confirm whether the 3D porous structure still remains for robust mechanical and electrical support after cycling, we have investigated the morphology and structure of cycled 3D porous Ni/Si electrode with SEM. One cell was disassembled after 100 cycles (charging up to 1.5 V) at a current density of 0.84 A g^{-1} for SEM characterization. As shown in Fig. 6, the morphology of the cycled Ni/Si electrode shows few variations compared to that of the pristine one. The gaps between each dendrite, composed of the porous wall, become distinct around 1–2 μm. And some crevices can be seen on the Si layer which covering the dendrite. But the film still keeps the 3D porous structure and each dendrite maintains its strong adhesion onto the Cu substrate. Under high magnification (Fig. 6b), although the surface of the Si layer becomes rough compared to pristine sample, the amorphous Si is not shed off. This morphology change is quite different from that of 200 nm-thick Si film deposited on smooth Cu foil, which mostly peeled off the substrate after 20 cycles [44].

Another advantage for the 3D porous Ni/Si electrode is its excellent rate performance. Fig. 7 shows the cycling performance of the 3D porous Ni/Si electrode at charge–discharge current densities of 4.2 A g^{-1} and 8.4 A g^{-1} for 100 cycles after being operated at 0.84 A g^{-1} for five cycles to activate the electrodes slowly as reported [28,29,45]. The phenomenon that the capacity first decreases and then increases is observed and also has reported by Guo's group [29] and Cui et al. [45]. The discharge capacity at 4.2 A g^{-1} rapidly declines to 1470 mAh g^{-1} at 3rd cycle and then gradually increases to 1640 mAh g^{-1} at 9th cycle and retains 1420 mAh g^{-1} after 100 cycles. The coulombic efficiency is over 99%. This phenomenon is more obvious at a charge–discharge

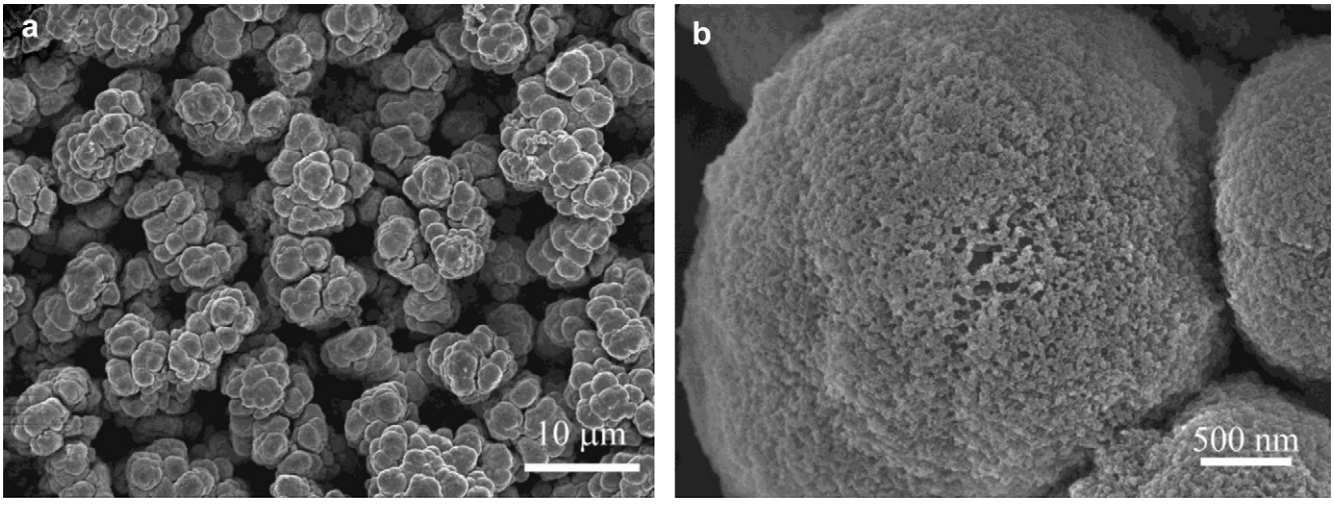

Fig. 6. (a) Ex situ SEM image of the fully discharged 3D porous Ni/Si electrode after 100 cycles, (b) high-magnification SEM image.

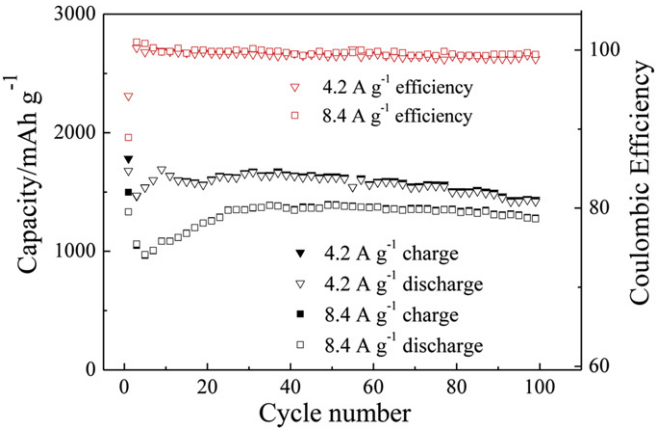

Fig. 7. Cycling behaviors of 3D porous Ni/Si electrode at charge–discharge current densities of 4.2 A g^{-1} and 8.4 A g^{-1} after activation for 5 cycles (0.84 A g^{-1}) with a cut-off voltage of 0.01–1.5 V.

current density of 8.4 A g^{-1}. The discharge capacity at 8.4 A g^{-1} declines to 972.5 mAh g^{-1} at the 5th cycle and then slowly increases to 1346 mAh g^{-1}. The capacity maintains a high value of 1273 mAh g^{-1} after 100 cycles. High coulombic efficiencies (over 99.3%) are observed as well. It is worth noting that it takes around 10 min to charge/discharge the 3D porous Ni/Si electrode at 8.4 A g^{-1}. This completely off-scale of time is due to the significant lower capacity compared to the theoretical capacity of Si.

The excellent electrochemical performance of the 3D porous Ni/Si as lithium-ion battery anode is attributed to its unique 3D porous structure. Periodic macroporous substrate/silicon structure films provide several advantages when used as lithium-ion battery electrodes. Firstly, macroporosity helps to accommodate volume swings during cycling without losing the structural integrity of the electrode and enables easy infiltration of electrolyte and fast liquid-phase lithium diffusion, reducing the concentration polarization and increasing rate performance and capacity of the cell. Secondly, the continuous 3D porous nano-Ni provides better electrical conductivity than aggregates of loosely connected particles and smooth films, which improves the rate capabilities of the electrodes. Thirdly, the large surface area provides more active sites for electrochemical reactions and leading to faster kinetics and higher utilization of active material.

4. Conclusions

In summery, a 3D porous Ni/Si composite film was synthesized through simple two steps. In this process, the 3D porous nano-Ni film is first synthesized on Cu substrate via hydrogen bubble template electrodeposition, and then amorphous silicon is deposited directly on 3D porous nano-Ni film by RF magnetron sputtering. The 3D porous Ni/Si composite film shows superior cycling stability and excellent rate capability, which are attributed to its unique 3D porous structure. Periodic macroporous substrate/silicon structure seems to be a promising material architecture for fundamental scientific explorations of a new genre of battery electrode materials.

Acknowledgments

The authors would like to acknowledge financial support from China Postdoctoral Science Foundation (Grant No. 20100481401), Zhejiang Province Education Department Scientific Research Project (Y201119640), the Fundamental Research Funds for the Central Universities (2011QNA4006) and Key Science and Technology Innovation Team of Zhejiang Province (2010R50013).

References

[1] P. Simon, Y. Gogotsi, Nat. Mater. 7 (2008) 845–854.
[2] A.S. Arico, P. Bruce, B. Scrosati, J.M. Tarascon, W. Van Schalkwijk, Nat. Mater. 4 (2005) 366–377.
[3] Y.G. Guo, J.S. Hu, L.J. Wan, Adv. Mater. 20 (2008) 2878–2887.
[4] P.I. Cowin, C.T.G. Petit, R. Lan, J.T.S. Irvine, S.W. Tao, Adv. Energy Mater. 1 (2011) 314–332.
[5] J.M. Tarascon, M. Armand, Nature 414 (2001) 359–367.
[6] X.H. Huang, J.P. Tu, Z.Y. Zeng, J.Y. Xiang, X.B. Zhao, J. Electrochem. Soc. 155 (2008) A438–A441.
[7] J.Y. Xiang, J.P. Tu, Y.F. Yuan, X.H. Huang, Y. Zhou, L. Zhang, Electrochem. Commun. 11 (2009) 262–265.
[8] A. Magasinski, P. Dixon, B. Hertzberg, A. Kvit, J. Ayala, G. Yushin, Nat. Mater. 9 (2010) 353–358.
[9] C.M. Park, J.H. Kim, H. Kim, H.J. Sohn, Chem. Soc. Rev. 39 (2010) 3115–3141.
[10] H.K. Liu, Z.P. Guo, J.Z. Wang, K. Konstantinov, J. Mater. Chem. 20 (2010) 10055–10057.
[11] Z.Y. Zeng, J.P. Tu, Y.Z. Yang, J.Y. Xiang, X.H. Huang, F. Mao, M. Ma, Electrochim. Acta 53 (2008) 2724–2728.
[12] P. Cu, R. Cai, Y.K. Zhou, Z.P. Shao, Electrochim. Acta 55 (2010) 3876–3883.
[13] D.Q. Shi, J.P. Tu, Y.F. Yuan, H.M. Wu, Y. Li, X.B. Zhao, Electrochem. Commun. 8 (2006) 1610–1614.
[14] H.-Y. Lee, Y.-L. Kim, M.-K. Hong, S.-M. Lee, J. Power Sources 141 (2005) 159–162.
[15] Z. Edfouf, F. Cuevas, M. Latroche, C. Georges, C. Jordy, T. Hézèque, G. Caillon, J.C. Jumas, M.T. Sougrati, J. Power Sources 196 (2011) 4762–4768.
[16] Z.Y. Zeng, J.P. Tu, X.L. Wang, X.B. Zhao, J. Electroanal. Chem. 616 (2008) 7–13.
[17] J.C. Guo, X.L. Chen, C.S. Wang, J. Mater. Chem. 20 (2010) 5035–5040.
[18] L. Su, Z. Zhou, M. Ren, Chem. Commun. 46 (2010) 2590–2592.
[19] C.K. Chan, H. Peng, G. Liu, K. Mcllwrath, X.F. Zhang, R.A. Huggins, Y. Cui, Nat. Nanotechnol. 3 (2008) 31–35.
[20] C.K. Chan, R.N. Patel, M.J. O'Connell, B.A. Korgel, Y. Cui, ACS Nano 4 (2010) 1443–1450.
[21] H. Chen, Y. Xiao, L. Wang, Y. Yang, J. Power Sources 196 (2011) 6657–6662.
[22] L.F. Cui, Y. Yang, C.M. Hsu, Y. Cui, Nano Lett. 9 (2009) 3370–3374.
[23] X. Chen, K. Gerasopoulos, J. Guo, A. Brown, C. Wang, R. Ghodssi, J.N. Culver, ACS Nano 4 (2010) 5366–5372.
[24] M.-H. Park, M.G. Kim, J. Joo, K. Kim, J. Kim, S. Ahn, Y. Cui, J. Cho, Nano Lett. 9 (2009) 3844–3847.
[25] T. Song, J. Xia, J.-H. Lee, D.H. Lee, M.-S. Kwon, J.-M. Choi, J. Wu, S.K. Doo, H. Chang, W.I. Park, D.S. Zang, H. Kim, Y. Huang, K.-C. Hwang, J.A. Rogers, U. Paik, Nano Lett. 10 (2010) 1710–1716.
[26] L. Hu, H. Wu, Y. Gao, A. Cao, H. Li, J. McDough, X. Xie, M. Zhou, Y. Cui, Adv. Energy Mater. 1 (2011) 523–527.
[27] A. Esmanski, G.A. Ozin, Adv. Funct. Mater. 19 (2009) 1999–2010.
[28] S.C. Zhang, Z.J. Du, R.X. Lin, T. Jiang, G.R. Liu, X.M. Wu, D.S. Weng, Adv. Mater. 22 (2010) 5378–5382.
[29] F.-F. Cao, J.-W. Deng, S. Xin, H.-X. Ji, O.G. Schmidt, L.-J. Wan, Y.-G. Guo, Adv. Mater. 23 (2011) 4415–4420.
[30] H.C. Shin, J. Dong, M.L. Liu, Adv. Mater. 15 (2003) 1610–1614.
[31] Y. Li, W.Z. Jia, Y.Y. Song, X.H. Xia, Chem. Mater. 19 (2007) 5758–5764.
[32] H.C. Shin, M.L. Liu, Chem. Mater. 16 (2004) 5460–5464.
[33] X.H. Xia, J.P. Tu, Y.Q. Zhang, Y.J. Mai, X.L. Wang, C.D. Gu, X.B. Zhao, J. Phys. Chem. C 115 (2011) 22662–22668.
[34] T. Karabacak, C.R. Picu, J.J. Senkevich, G.C. Wang, T.M. Lu, J. Appl. Phys. 96 (2004) 5740–5746.
[35] Y.X. Yin, S. Xin, L.J. Wan, C.J. Li, Y.G. Guo, J. Phys. Chem. C 115 (2011) 14148–14154.
[36] K.L. Lee, J.Y. Jung, S.W. Lee, H.S. Moon, J.W. Park, J. Power Sources 129 (2004) 270–274.
[37] M.K. Datta, J. Maranchi, S.J. Chung, R. Epur, K. Kadakia, P. Jampani, P.N. Kumta, Electrochim. Acta 56 (2011) 4717–4723.
[38] V. Baranchugov, E. Markevich, E. Pollak, G. Salitra, D. Aurbach, Electrochem. Commun. 9 (2007) 796–800.
[39] H. Kim, J. Cho, Nano Lett. 8 (2008) 3688–3691.
[40] K.F. Chiu, K.M. Lin, H.C. Lin, C.H. Hsu, C.C. Chen, D.T. Shieh, J. Electrochem. Soc. 155 (2008) A623–A627.
[41] X.H. Huang, J.P. Tu, X.H. Xia, X.L. Wang, J.Y. Xiang, L. Zhang, J. Power Sources 195 (2010) 1207–1210.
[42] J.L. Gomez-Camer, J. Morales, L. Sanchez, J. Mater. Chem. 21 (2011) 811–818.
[43] H. Kim, B. Han, J. Choo, J. Cho, Angew. Chem. Int. Ed. 47 (2008) 10151–10154.
[44] J.P. Maranchi, A.F. Hepp, A.G. Evans, N.T. Nuhfer, P.N. Kumta, J. Electrochem. Soc. 153 (2006) A1246–A1253.
[45] L.F. Cui, R. Ruffo, C.K. Chan, H.L. Peng, Y. Cui, Nano Lett. 9 (2009) 491–495.